November 08, 2006

A study of anodization process during pore formation in nanoporous alumina templates

Z. Wu
Northeastern University

C. Richter
Northeastern University

L. Menon
Northeastern University

A Study of Anodization Process during Pore Formation in Nanoporous Alumina Templates

Z. Wu, C. Richter and L. Menon

J. Electrochem. Soc. 2007, Volume 154, Issue 1, Pages E8-E12.
doi: 10.1149/1.2382671

Journal of The Electrochemical Society, **154** (1) E8-E12 (2007)
0013-4651/2006/154(1)/E8/5/$20.00 © The Electrochemical Society

A Study of Anodization Process during Pore Formation in Nanoporous Alumina Templates

Z. Wu,[a] C. Richter,[b] and L. Menon[a,z]

[a]*Department of Physics and* [b]*Department of Chemical Engineering, Northeastern University, Boston, Massachusetts 02115, USA*

We have carried out a systematic investigation of the anodization procedure in order to determine the exact chemical mechanism of the dissolution process responsible for pore formation in nanoporous alumina templates. We measured the anodization current as a function of time and compared it with the thickness of porous aluminum oxide layer obtained from cross-section scanning electron microscopy images. From this, we calculated the number of moles of electrons generated per mole of porous alumina grown. This analysis is consistent with a reaction mechanism in which aluminum is converted to aluminum oxide in addition with the direct transfer of aluminum ions across the thin barrier aluminum oxide into the electrolyte. Hence, experimental evidence is reported that indicate that the dissolution process observed is that of Al^{3+} ions migrating across the barrier layer and dissolving into the solution. Contrary to the suggestion of some authors, these experiments indicate that at most a negligible amount of oxide dissolves during the anodization of aluminum.
 [DOI: 10.1149/1.2382671]

Manuscript submitted June 13, 2006; revised manuscript received August 7, 2006. Available electronically November 8, 2006.

Nanoporous alumina templates are aluminum oxide films consisting of nanosized cylindrical pores arranged parallel to each other in a quasihexagonal arrangement. Such templates have been intensely researched due to their wide-spread application in nanofabrication.[1-5] The templates are prepared by means of an anodization process—the electrochemical oxidation of aluminum film in an acid under dc conditions. Pore parameters (diameter, length) are determined largely by the anodization conditions, such as the applied dc voltage, pH of the acid, time of anodization, etc.[6-8] Currently, there is only limited theoretical understanding of the pore formation in these templates.[9-13] In this paper, a set of experiments that were specifically designed to reveal the exact mechanism of oxide dissolution are described.

Although existing theories differ (see, for example, Ref. 9-13) regarding the chemical and physical details of the anodization process there exist a consensus that pores form as a result of competing oxidation and dissolution processes. This understanding, as first formulated in the widely referenced work of Thompson et al.[14] Shingubara,[15] and O'Sullivan,[9] suggests that oxidation and dissolution proceed by the following mechanisms: (*i*) the growth of aluminum oxide, either at the interface between aluminum and alumina or within the barrier layer due to the countermigration of Al^{3+} ions and OH^- and O^{2-} ions; and (*ii*) the dissolution of aluminum oxide at the interface between the alumina film and solution. Written in terms of their chemical reactions these two processes are most commonly formulated as:

Formation of aluminum oxide

$$2Al(s) + 3H_2O \rightarrow Al_2O_3(s) + 6H^+(aq) + 6e^- \quad [1]$$

Dissolution of aluminum oxide

$$Al_2O_3(s) + 6H^+(aq) \rightarrow 2Al^{3+}(aq) + 3H_2O \quad [2]$$

Recognizing that these processes involve the counterdiffusion of oxide carrying and Al ions[9,16] some authors[17-19] suggested that field-assisted dissolution may also occur by the following pathway (illustrated in Fig. 1).

Net diffusion of Al^{3+} across barrier layer

$$Al(s) \rightarrow Al^{3+}(aq) + 3e^- \quad [3]$$

with the understanding that the electrons are transferred directly to species in the electrolyte,[20] for instance by proton reduction.[21]

Net diffusion of Al^{3+} across barrier

$$3H^+(aq) + Al(s) \rightarrow Al^{3+}(aq) + \frac{3}{2}H_2 \quad [4]$$

In this work, we have carried out a systematic investigation of the anodization process as a function of time in order to measure the relative contributions of the different chemical mechanisms proposed for the field assisted etching of alumina pores. Our results are discussed below.

The experimental setup for anodization of Al foils has been reported earlier.[22] A brief description is provided here. Anodization is carried out in a commercially available electrochemical flat cell. A Pt mesh acts as cathode while aluminum film acts as anode. In our experiments, we have used sputtered Al films on the surface of Si wafers as the anode. Thickness of the Al film is ~350 nm. Such thin films were intentionally used for this work, since we are interested in studying the anodization process from start to finish (when all the aluminum is converted to aluminum oxide). We started with a 2 in. diameter Si wafer with a uniformly deposited 350 nm thick layer of Al. The wafer was diced into several 1.5 cm square pieces. Anodization of the Al film for each of these pieces was carried out in 3% oxalic acid at 40 V. The samples were anodized for varying lengths of time ranging from 1 to 50 s to study the initial formation of the oxide layer. To study steady state oxidation and dissolution 1.5 cm

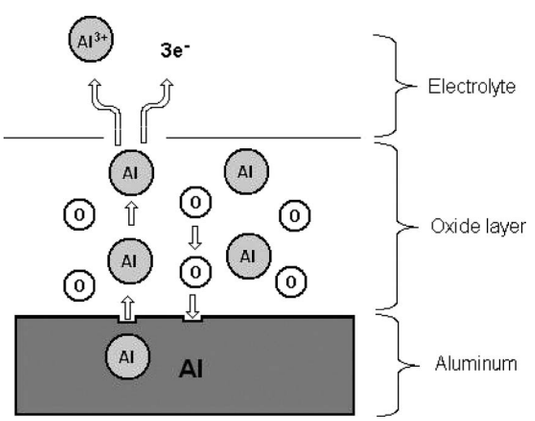

Figure 1. A schematic representation of the field-induced counterdiffusion of aluminum and oxygen atoms (or ions). Also indicated is the dissolution of aluminum ions into the electrolyte according to the mechanism of Eq. 3 (i.e., there is no net oxygen dissolution). Oxidation of alumina occurs at the oxide layer–aluminum interface.

[z] E-mail: l.menon@neu.edu

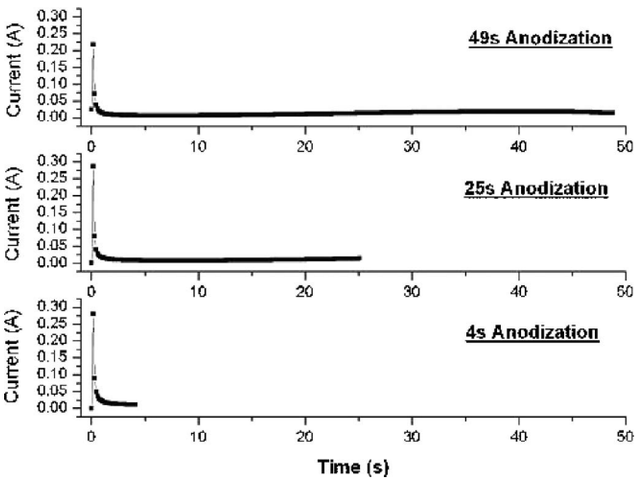

Figure 2. Anodization current as a function of time for three representative samples with anodization times 4 s, 25 s, and 49 s.

square pieces of 0.25 mm aluminum foil (Alfa Aesar 99.997% pure) was anodized in 3% oxalic acid at 40 V and 60 V. Samples were anodized for time intervals ranging from 30 min to 4 h. The anodization current as a function of time was recorded using a power supply (Agilent 6811B) interfaced with a computer. The current versus time data for some of the samples are shown in Fig. 2. In each of these experiments the sample size, thickness of Al film, and distance between electrodes was maintained constant. Hence, the net current as a function of time is the same for all of these samples. The current is first found to rise during the first 100 ms. It reaches a maximum value of about 1.2 A, after which it drops quickly to around 6 mA and then rises slightly and remains more or less constant at around 19 mA. At 49 s the current is found to drop sharply indicating conversion of the entire Al film into aluminum oxide.

Figure 3 shows the cross-sectional scanning electron microscopy (SEM) image of the samples as a function of anodization time. All the SEM images are recorded under the same magnification condition so that the thickness of the various layers may be directly compared. The initial thickness (at 0 s) of the Al foil is seen to be around 350 nm. With increasing anodization time, the thickness of Al is seen to drop as Al is converted into porous Al_2O_3, which sits atop the Al film. As expected, cylindrical pores arranged parallel to each other are seen with increasing anodization time (Fig. 3a and clarified in Fig. 3b). The porous layer is open at the top and is separated from the remaining Al by a U-shaped barrier layer of aluminum oxide (clarified in Fig. 3c). Exchange of ions happens across this thin barrier oxide layer.

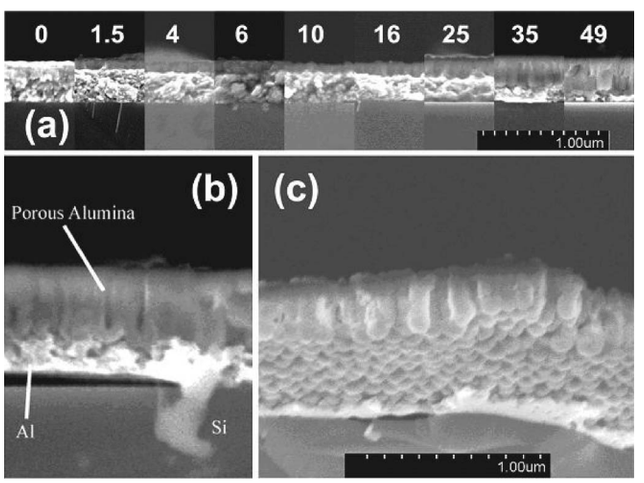

Figure 3. (a) Cross-section scanning electron microscopy images of samples anodized for varying times ranging from 1 to 49 s. (b) Magnified image showing pore structure for a sample anodized for 35 s. (c) Scanning electron microscopy images of samples anodized for 49 s under 40 V showing the U-shape bottom that suggest that the relatively short time anodization is sufficient to form a fully developed pore structure.

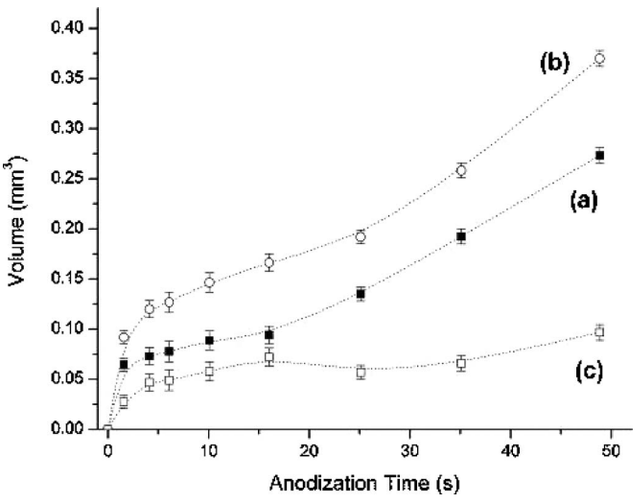

Figure 4. (a) Volume of porous oxide layer (observed) as a function of anodization time. (b) Hypothetical volume of oxide layer (calculated) in the absence of dissolution as a function of time. (c) Calculated volume of dissolved oxide layer as a function of time-difference between curve a and b. Note: It turned out that the mechanism suggested by this representation of the data (hypothetical curves b and c) does not fit the current data. In essence, the total time integrated amount of oxide suggested by curve b was never formed and the oxide dissolution suggested by curve c never happened. Instead, dissolution was merely that of Al^{3+} ions with no net amount of oxygen returning to the solution.

From the SEM images, the thickness of the porous Al_2O_3 layer is found to increase as a function of anodization time. Finally, for the sample anodized for 49 s almost all the aluminum is seen to be converted to aluminum oxide in consistence with the current data. From the images, we measured the thickness of the porous oxide layer (L_T), the thickness of the remaining Al film and the thickness of the barrier layer (L_B) as a function of anodization time. From a digital pixel analysis of top-view SEM images, the ratio of the area of the pores to the total area of the sample (R) was calculated to be 0.196. Using these measurements the volume of the porous aluminum oxide was calculated using the following formula

$$\text{Volume} = L_B \times A + (1 - R)(L_T - L_B)$$

where A is the total anodized area of the sample. This volume, which is the net result of both the oxidation and the dissolution processes, is shown in Fig. 4 (curve a). From the measurement of the drop in Al film thickness the total number of moles of Al that have been consumed up till every time step was calculated. In the absence of dissolution we would expect all of this Al to be converted to a thick oxide layer. Using this information the volume of the aluminum oxide that would have been present had there been no dissolution can be estimated by multiplying the number of moles of Al consumed by the molar volume of Al_2O_3 (volume of Al_2O_3/mole Al). This hypothetical volume of aluminum oxide is also plotted in Fig. 4 (curve b). Subtracting curve a from curve b, we can estimate the volume of aluminum oxide layer dissolved as a function of time assuming the mechanism of Eq. 2. This is plotted as curve c. By a

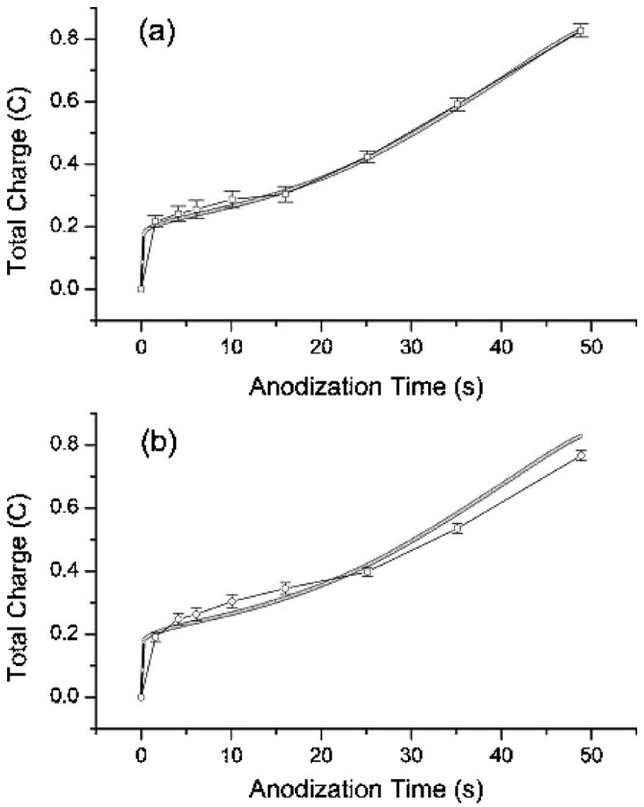

Figure 5. (a) Integrated current (thick line) plotted together with a rescaling of curve 4a (thin line with symbols). Note that these two curves are in extremely close agreement even though they represent data from very different measurements. The integrated current is recorded by the power supply while the scaled oxide layer thickness is the result of thickness measurements based on SEM cross-section images and subsequent analysis. (b) The hypothetical oxide curve (curve b, Fig. 4) optimally scaled to fit the integrated current curve. Clearly, this fit is markedly inferior to the fit in Fig. 5a. If oxide dissolution occurred according to the mechanism of equation 2, then it should be curve 4b and not 4a (as was used in Fig. 5a) that scale with the integrated current curve. This is so because curve 4b represents the total amount of oxygen that oxidized Al up till time t according to mechanism 2. A comparison of Figs. 5a and b clearly suggest the mechanism of Eq. 3 over that of Eq. 2.

similar calculation the volume of Al dissolved assuming the mechanism of Eq. 3 can be calculated.

Thus, through our analysis we have effectively quantified the oxidation and dissolution processes during anodization. It can be inferred from Fig. 4 that the oxidation process dominates the dissolution process for thin aluminum films as studied in the present experiment.

In order to compare the thickness information from the SEM analysis with the current recorded in the external circuit, we have carried out the following analysis. First, we integrated the anodization current curve (Fig. 2) over the anodization time. Upon integration, one obtains the total charge transferred through the external circuit until any given time *t*. The integrated current curve is shown in Fig. 5a (thick line). We found a very close fit of this curve (Fig. 5a) to the curve tracing out the physically observed volume of the porous layer (Fig. 4a) upon merely multiplying the latter by a constant factor (shown by the thin line in curve 5a). This result can be given physical meaning as follows. By multiplying curve 4a (observed volume of porous Al_2O_3 [vol]) by the molar density of O atoms in Al_2O_3 [mol/vol] one can see that curve 4a is proportional to the number of O atoms present in oxidized Al_2O_3 at any given time. The fact that this curve scales with the integrated current in the external circuit suggests that: (*i*) the number of electrons transferred around the external circuit is proportional to the number of oxygen atoms that formed Al_2O_3 until that time; and (*ii*) the number of oxygen atoms that oxidized Al until any given time is equal to the number of oxygen atoms observed in Al_2O_3 at that given time. The first point is in accordance with the mechanisms of both Eq. 2 and 4 since for both mechanisms there is no external "dissolution current." That is, these dissolution reactions as written only involve electron transfer directly to the electrolyte (most likely through anodic proton reduction) and not through the external circuit. Hence, the suggested chemistry supports the finding that oxidation alone determines the external current load. The second point on the other hand is only (refer to caption to Fig. 5b) in accordance with the mechanism of Eq. 3 and 4. This result suggests that very little oxygen dissolves back into the electrolyte once it has been incorporated into the oxide layer. Although this result was not anticipated it should perhaps not be surprising considering the large affinity of aluminum for oxidation by oxygen ($\Delta H_{Al_2O_3} = -1675.7$ kJ/mol).

Table I. Proportionality constant comparing the number of electrons transferred around the external circuit for each mole of Al_2O_3 formed until the time listed in column 1. In the second column this calculation was done assuming the mechanism of Eq. 2 and in the third column based on the mechanism of Eq. 3.

Time (s)	Number of moles of electrons transferred in the external circuit per mole of Al_2O_3 formed-calculation based on	
	Mechanism (2)	Mechanism (3)
1.58	6.24	9.65
4.13	5.34	9.65
6.09	5.33	9.65
10.08	5.20	9.65
16.00	4.83	9.65
25.11	5.84	9.65
35.11	6.06	9.64
48.84	5.92	9.64

The proportionality constant for the scaling shown in Fig. 5a is calculated to be 36.41 C/mm^3, which translates to 9.6 mol of electrons transferred around the external circuit per mol of porous alumina formed. The oxidation reaction as written in Eq. 1, involves a charge transfer of 6 mol of electrons around the external circuit for every mole of Al_2O_3 formed. The additional electrons are most likely due to side reactions of which oxygen evolution at the anode is probably the most prominent. It is also possible that a minor fraction of the dissolution current (electrons on the right side of Eq. 3) are not consumed by reactions like anodic proton reaction and therefore may contribute towards the extra electrons that was observed in the external current.

In Table I we have calculated the proportionality constant for six individual data points. That is, we have calculated the average rate of electrons transferred around the external circuit for each mole of Al_2O_3 formed (by incorporating O atoms or ions from the electrolyte) until the time listed in column 1. In the second column this calculation was done assuming the mechanism of Eq. 2 and in the third column based on the mechanism of Eq. 3 and 4. The unexpected finding that curve 4a scales with curve 5a is reflected by the fact that the proportionality constant in the third column is nearly constant. The result found in the third column is remarkable considering that the two sets of data showing this high degree of continued coincidence (or fixed proportionality) come from very different measurements; current as recorded by a current meter and oxide and aluminum volumes based on the analyses of high-quality SEM images. Since side reactions could conceivably be independent of oxidation rates the existence of such a constant ratio between the observed alumina volume and the number of electrons traversing the external is not a theoretical necessity. Finally, recall that the mechanism of Eq. 2 requires six electrons to be passed from the anode to

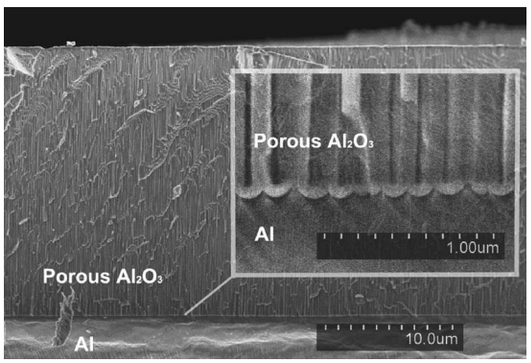

Figure 6. Cross-sectional scanning electron microscopy images of samples anodized for 30 min under 60 V and magnified inset images showing the U-shaped barrier layer interface between Al and porous Al_2O_3.

the cathode. Now, it can be seen in column two that the ratio of electrons to Al_2O_3 formed falls as low as ~4.8 when the calculation of this ratio is based on the mechanism of Eq. 2. This contradiction firmly rules out the possibility that the mechanism of Eq. 2 can be solely responsible for anodic dissolution. If we combine this observation with the data in column three that seems to indicate that the mechanism of Eq. 3 and 4 alone sets the pace for external electron transfer we are lead to the hypothesis that only the mechanism of Eq. 3 and 4 was active, at least to a measurable degree, in these experiments.

It is desirable to investigate to what degree these results carry over to longer anodization as is, typically, done in the case of thicker

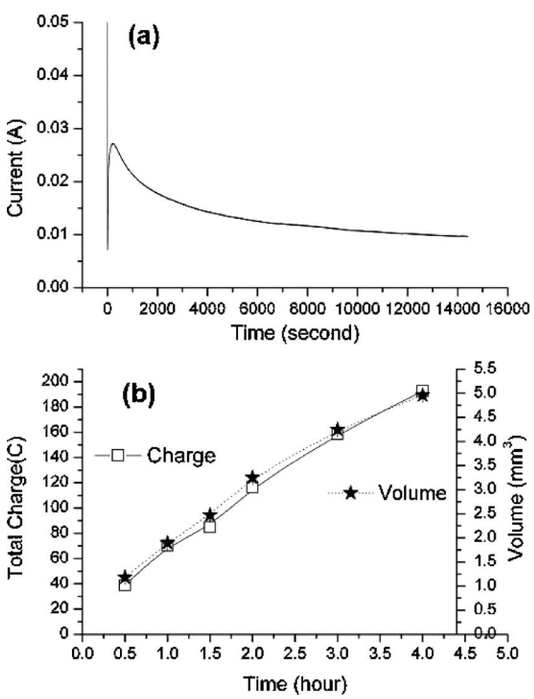

Figure 7. (a) Anodization current versus time for 0.25 mm thick aluminum foil. It can be seen that the total amount of current transferred through the external circuit steadily levels off to an asymptotic steady state value. (b) The dashed line (star symbols) is a rescaling of oxide layer volume data (similar to that of Fig. 4a) for anodization done at 60 V over longer time periods. This curve follows the integrated current curve (solid line and square symbols) closely, as was the case with shorter anodization times. The scaling constant translates into 9.0 mol of electrons per mol of Al_2O_3 formed.

commercially available aluminum foils. Toward that end the analysis described above was repeated for anodization at 40 V and 60 V over periods of time ranging from 30 min and 4 h (see Fig. 6). It is expected that the oxidation process will slow down as the thickness of the porous oxide layer is increased. This is supported by the current data for these samples, an example of which is shown in Fig. 7a. As can be seen in Fig. 7b, the analysis for these thicker samples that were anodized over longer periods of time, also lead to an excellent fit between the observed oxide film thickness and the integrated current curve. The optimal scaling constant in the 40 V case turned out to be 9.4 and in the 60 V case 9.0. The lower number of electrons in the 40 V case may perhaps be due to the fact that a thinner barrier layer was observed to exist at lower voltages. A thinner barrier layer theoretically increases the electron current that facilitate the oxygen evolution side reaction. The fact that the short time anodization (at 40 V) gave an even greater number of excess electrons also fit this theory—during the first few seconds of anodization there is a very thin oxide layer which may well facilitate a relatively large oxygen evolution side reaction.

In conclusion, we have investigated anodization process in thin aluminum films sputtered on Si wafers for an acidic electrolyte, namely, 3% oxalic acid. We measured anodization current and thickness of aluminum and aluminum oxide layers in porous alumina templates as a function of time. An analysis of these measurements leads to the empirically supported conclusion that the mechanism implied by Eq. 2 plays at best a minor role under the conditions investigated here. Hence, these experiments show that the chemistry that was first tentatively proposed by Diggle et al.,[17] and subsequently most frequently suggested as the mechanism responsible for dissolution during aluminum oxidation[15,19,23,24] may not be operative to a measurable degree. Instead, the mechanism of Eq. 3 and 4 was strongly implicated as being responsible for the "ejection of Al^{3+} ions into the electrolyte," as was suggested by O'Sullivan[9] and Thompson et al.[14] almost 30 years ago. Our experiments also suggest that the number of electrons that traverse the external circuit for every mole of porous alumina growth is typically around 9 to 10 mol. The proposed oxidation chemistry suggests that six of these are generated in the oxidation process with the remainder most likely being generated in side reactions like oxygen evolution.

Acknowledgment

This work is supported by NSF CAREER Grant No. ECS-0551468.

Northeastern University assisted in meeting the publication costs of this article.

References

1. L. Menon, in *Dekker Encyclopedia of Nanoscience and Nanotechnology*, J. A. Schwarz, Editor, Marcel Dekker, New York (2004).
2. L. Menon, K. B. Ram, S. Patibandla, D. Aurongzeb, M. Holtz, J. Yun, V. Kuryatkov, and K. Zhu, *J. Electrochem. Soc.*, **151**, C492 (2004).
3. K. Nielsch, J. Choi, K. Schwirn, R. B. Wehrspohn, and U. Gosele, *Nano Lett.*, **2**, 677 (2002).
4. H. Zeng, M. Zheng, R. Skomski, D. J. Sellmyer, Y. Liu, L. Menon, and S. Bandyopadhyay, *J. Appl. Phys.*, **87**, 4718 (2000).
5. F. Li and R. M. Metzger, *J. Appl. Phys.*, **81**, 3806 (1997).
6. H. Masuda and K. Fukuda, *Science*, **268**, 1466 (1995).
7. A. P. Li, F. Muller, and U. Gosele, *Electrochem. Solid-State Lett.*, **3**, 131 (2000).
8. D. AlMawlawi, N. Coombs, and M. Moskovits, *J. Appl. Phys.*, **70**, 4421 (1991).
9. J. P. W. O'Sullivan and G. C. Wood, *Proc. R. Soc. London, Ser. A*, **317**, 511 (1970).
10. O. Jessensky, F. Muller, and U. Gosele, *Appl. Phys. Lett.*, **72**, 1173 (1998).
11. V. P. Parkhutik and V. I. Shershulsky, *J. Phys. D*, **25**, 1258 (1992).
12. E. Palibroda, A. Lupsan, S. Pruneanu, and M. Savos, *Thin Solid Films*, **256**, 101 (1995).
13. G. K. Singh, A. A. Golovin, and I. S. Aranson, *Phys. Rev. B*, **73**, 205422 (2006).
14. G. E. Thompson, R. C. Furneaux, G. C. Wood, J. A. Richardson, and J. S. Goode, *Nature (London)*, **272**, 433 (1978).
15. S. Shingubara, *J. Nanopart. Res.*, **5**, 17 (2003).
16. J. A. Davies, B. Domeij, J. P. S. Pringle, and F. Brown, *J. Electrochem. Soc.*, **112**, 675 (1965).
17. J. W. Diggle, T. C. Downie, and C. W. Goulding, *Chem. Rev. (Washington, D.C.)*, **69**, 365 (1969).
18. T. Valand and K. E. Heusler, *J. Electroanal. Chem. Interfacial Electrochem.*, **149**, 71 (1983).

19. L. Menon, in *Advances in Nanophase Materials and Nanotechnology (Quantum Dots and Nanowires)*, S. Bandyopadhyay and H. S. Nalwa, Editors, American Scientific Publishers, Stevenson Ranch, CA (2003).
20. R. T. Foley and T. H. Nguyen, *J. Electrochem. Soc.*, **129**, 464 (1982).
21. F. Li, L. Zhang, and R. M. Metzger, *Chem. Mater.*, **10**, 2470 (1998).
22. V. Sadasivan, C. P. Richter, L. Menon, and P. F. Williams, *AIChE J.*, **51**, 649 (2005).
23. S. Bandyopadhyay, A. E. Miller, H. C. Chang, G. Banerjee, V. Yuzhakov, D. F. Yue, R. E. Ricker, S. Jones, J. A. Eastman, E. Baugher, and M. Chandrasekhar, *Nanotechnology*, **7**, 360 (1996).
24. G. Q. Ding, M. J. Zheng, W. L. Xu, and W. Z. Shen, *Nanotechnology*, **16**, 1285 (2005).